arXiv:physics/0007041v2 [physics.geo-ph] 25 Jan 2001

The shock-acoustic waves generated by earthquakes

Afraimovich E. L., Perevalova N. P., Plotnikov A. V., Uralov A. M.

Institute of Solar-Terrestrial Physics SD RAS,

p. o. box 4026, Irkutsk, 664033, Russia

fax: +7 3952 462557; e-mail: afra@iszf.irk.ru

Abstract

We investigate the form and dynamics of shock-acoustic waves generated by earthquakes. We use the method for detecting and locating the sources of ionospheric impulsive disturbances, based on using data from a global network of receivers of the GPS navigation system and requiring no a priori information about the place and time of associated effects. The practical implementation of the method is illustrated by a case study of earthquake effects in Turkey (August 17, and November 12, 1999), in Southern Sumatera (June 4, 2000), and off the coast of Central America (January 13, 2001). It was found that in all instances the time period of the ionospheric response is 180-390 s, and the amplitude exceeds by a factor of two as a minimum the standard deviation of background fluctuations in total electron content in this range of periods under quiet and moderate geomagnetic conditions. The elevation of the wave vector varies through a range of 20-44°, and the phase velocity (1100-1300 m/s) approaches the sound velocity at the heights of the ionospheric F-region maximum. The calculated (by neglecting refraction corrections) location of the source roughly corresponds to the earthquake epicenter. Our data are consistent with the present views that shock-acoustic waves are caused by a piston-like movement of the Earth surface in the zone of an earthquake epicenter.

1 Introduction

A plethora of publications have been devoted to the study of the ionospheric response to disturbances arising from impulsive forcing on the Earth's atmosphere. It was found that in many cases a high proportion of the energy of the initial atmospheric disturbance is concentrated in the acoustic shock wave. Large earthquakes also provide a natural source of impulsive forcing.

These investigations have also important practical implications since they furnish a means of substantiating reliable signal indications of technogenic effects (among them, unauthorized), which is necessary for the construction of an effective global radiophysical system for detection and localization of these effects. Essentially, existing global systems of such a purpose use different processing techniques for infrasound and seismic signals. However, in connection with the expansion of the geography and of the types of technogenic impact on the environment, very challenging problems heretofore have been those to improve the sensitivity of detection and the reliability of measured parameters of the sources of impacts, based also on using independent measurements of the entire spectrum of signals generated during such effects.

To solve the above problems requires reliable information about fundamental parameters of the ionospheric response to the shock wave, such as the amplitude and the form, the period, the phase and group velocity of the wavetrain, as well as angular characteristics of the wave vector. Note that for naming the ionospheric response of the shock wave, the literature uses terminology incorporating a different physical interpretation, among them the term 'shock-acoustic wave' (SAW) (Nagorsky, 1998). For convenience, in this paper we shall use this term despite the fact that it does not reflect essentially the physical nature of the phenomenon.

There is a wide scatter of published data on the main parameters of SAWs generated during industrial explosions and earthquakes. The oscillation period of the ionospheric response of SAWs varied from 30 to 300 sec., and the propagation velocity fluctuated from 700 to 1200 m/s (Nagorsky, 1998; Fitzgerald, 1997; Calais et al., 1998; Afraimovich et al., 1984; Blanc and Jacobson, 1989).

The lack of comprehensive, reliable data on SAW parameters is due primarily to the limitations of existing experimental methods and detection facilities. The main body of data was obtained by measuring the frequency Doppler shift at vertical and oblique-incidence ionospheric soundings in the HF range (Nagorsky, 1998; Afraimovich et al., 1984; Jacobson and Carlos, 1994). In some instances the sensitivity of this method is sufficient to detect the SAW reliably; however, difficulties emerge for localizing the region where the detected signal is generated. These problems are caused by the multiple-hop character of HF signal propagation. This gives no way of deriving reliable information about the phase and group velocities of the SAW propagation, estimating angular characteristics of the wave vector, and, further still, of localizing the SAW source.

Using the method of transionospheric sounding with VHF radio signals from geostationary satellites, a number of experimental data on SAW parameters were obtained in measurements of the Faraday rotation of the plane of signal polarization which is proportional to a total electron content (TEC) along the line connecting the satellite-borne transmitter with the receiver (Li et al., 1994).

A common drawback of the above-mentioned methods when determining the SAW phase velocity is the necessity of knowing the time of events since this velocity is inferred from the SAW delay with respect to the time of events assuming that the velocity is constant along the propagation path, which is quite contrary to fact.

For determining the above-mentioned rather complete set of SAW parameters, it is necessary to have appropriate spatial and temporal resolution which cannot be ensured by existing, very sparse, networks of ionosondes, oblique-incidence radio sounding paths, and incoherent scatter radars.

The advent of the Global Positioning System (GPS) plus the subsequent creation of extensive networks of GPS stations (at least 757 sites as of November 2000), with their data being now available via the Internet, opened up a new era in remote ionospheric sensing.

Currently some authors have embarked on an intense development of methods for detecting the ionospheric response of strong earthquakes (Calais and Minster, 1995), rocket launchings (Calais and Minster, 1996), and industrial surface explosions (Fitzgerald, 1997; Calais et al., 1998). In the cited references the SAW phase velocity was determined by the 'crossing' method by estimating the time delay of SAW arrival at subionospheric points corresponding to different GPS satellites observed at a given time. However, the accuracy of such a method is rather low because the altitude at which the subionospheric points are specified, is determined in a crude way.

The goal of this paper is to describe a method for determining parameters of the SAW generated by earthquakes (including the phase velocity, angular characteristics of the SAW wave vector, the direction towards the source, and the source location) using GPS-arrays whose elements can be chosen out of a large set of GPS stations from the global GPS network.

Section 2 presents a description of the experimental geometry, and general information about the earthquakes under consideration. The proposed method is briefly outlined in Section 3. Results of measurements of SAW parameters from different GPS arrays during earthquakes are presented in Section 4. Section 5 is devoted to the discussion of experimental results, including analytical simulation results.

2 The geometry and general characterization of experiments

Detection results on two earthquakes in Turkey (August 17, and November 12, 1999), in Southern Sumatera (June 4, 2000), and off the coast of Central America (January 13, 2001) are presented below. The information about the earthquakes, was acquired via the Internet 'http://earthquake.usgs.gov'. General information about these earthquakes is presented in Table 1 (including the time of the main shock t_0 in the universal time UT, the position of the earthquake epicenter, depth,

the magnitude, as well as the level of geomagnetic disturbance from the data on Dst-variations). It was found that the deviation of Dst for the selected days was quite moderate, which enabled the SAWs to be identified.

Fig. 1 illustrates the experimental geometry during the earthquakes in Turkey – a), off the coast of Central America – b), and in Southern Sumatera – c).

In spite of the small number of GPS stations in the earthquake area, we were able to use a sufficient number of them for the implementation of the proposed method.

Table 2 presents the geographic coordinates of the GPS stations used as GPS array elements.

3 Methods of determining shock-acoustic wave characteristics using GPS-arrays

The standard GPS technology provides a means for wave disturbances detecion based on phase measurements of TEC at each of spaced two-frequency GPS receivers. A method of reconstructing TEC variations was detailed and validated in a series of publications (Calais and Minster, 1995, 1996; Fitzgerald, 1997). We reproduce here only the final formula for the total electron content (I)

$$I = \frac{1}{40.308} \frac{f_1^2 f_2^2}{f_1^2 - f_2^2} [(L_1\lambda_1 - L_2\lambda_2) + const + nL] \qquad (1)$$

where $L_1\lambda_1$ and $L_2\lambda_2$ are additional paths of the radio signal caused by the phase delay in the ionosphere, (m); L_1 and L_2 represent the number of phase rotations at the frequencies f_1 and f_2; λ_1 and λ_2 stand for the corresponding wavelengths, (m); $const$ is the unknown initial phase ambiguity, (m); and nL are errors in determining the phase path, (m).

Phase measurements in the GPS can be made with a high degree of accuracy corresponding to the error of TEC determination of at least 10^{14} m^{-2} when averaged on a 30-second interval, with some uncertainty of the initial value of TEC, however. This makes possible detection of ionization irregularities and wave processes in the

ionosphere over a wide range of amplitudes (up to 10^{-4} of the diurnal TEC variation) and periods (from 24 hours to 5 min). The unit of TEC, $TECU$, is equal to 10^{16} m^{-2}, it is commonly accepted in the literature, and will be used in the following.

A convenient way of determining the ionospheric response delay of the shock wave involves the frequency Doppler shift F from TEC series obtained by formula (1). Such an approach is also useful in comparing TEC response characteristics from the GPS data with those obtained by analyzing VHF signals from geostationary satellites, as well as in detecting the shock wave in the HF range. To an approximation sufficient for the purpose of our investigation, a corresponding relationship was obtained by K. Davies (1969)

$$F = 13.5 \cdot 10^{-8} I'_t / f \tag{2}$$

where I'_t stands for the time derivative of TEC. Relevant results derived from analyzing the $F(t)$-variations calculated for the 'reduced' frequency of 136 MHz are discussed in Section 4.

The correspondence of space-time phase characteristics, obtained through transionospheric soundings, with local characteristics of disturbances in the ionosphere was considered in detail in a wide variety of publications (Afraimovich et al., 1992; Mercier and Jacobson, 1997) and is not analyzed at length in this study. The most important conclusion of the cited references is the fact that, as for the extensively exploited model of a 'plane phase screen' disturbances $\Delta I(x, y, t)$ of TEC faithfully copy the horizontal part of the corresponding disturbance of local electron concentration $\Delta N(x, y, z, t)$, independently of the angular position of the source, and can be used in experiments for measuring the TEC disturbances.

However, the TEC response amplitude experiences a strong azimuthal dependence caused by the integral character of a transionospheric sounding. As a first approximation, the transionospheric sounding method is responsive only to Traveling Ionospheric Disturbances (TIDs) with the wave vector K_t perpendicular to the direction r wich is along the Line-of-Sight (LOS) from the receiver to the satellite.

A corresponding condition for elevation θ and azimuth α of an arbitrary wave vector K_t normal to the direction r, has the form

$$\theta = \arctan(-\cos(\alpha_s - \alpha)/\tan\theta_s) \tag{3}$$

where α_s is the azimuthal angle measured east to north, and θ_s is the angle of elevation of the satellite at the receiver.

We used formula (3) to determine the elevation θ of K_t from the known mean value of azimuth α by Afraimovich et al. (1998) – see Sections 3.2 and 4.

3.1 Detection and determination of the horizontal phase velocity and the direction of the SAW phase front along the ground by GPS-arrays

In the simplest form, space-time variations of the TEC $\Delta I(t, x, y)$ in the ionosphere, at each given time t can be represented in terms of the phase interference pattern that moves without a change in its shape (the solitary, plane travelling wave)

$$\Delta I(t, x, y) = \delta \sin(\Omega t - K_x x - K_y y + \varphi_0) \tag{4}$$

where δ, K_x, K_y, Ω, are the amplitude, the x- and y-projections of the wave vector $\boldsymbol{K}$, and the angular frequency of the disturbance, respectively; $T = 2\pi/\Omega$, $\Lambda = 2\pi/|K|$ is its period and wavelength; and φ_0 is the initial phase of the disturbance. The vector K is a horizontal projection of the full vector K_t.

At this point, it is assumed that in the case of small spatial and temporal increments (the distances between GPS-array sites are less than the typical spatial scale Λ of TEC variation, and the time interval between counts is less than the corresponding time scale), the influence of second derivatives can be neglected. The following choices of GPS-arrays all meet these requirements.

We now summarize briefly the sequence of data processing procedures. Out of a large number of GPS stations, three sites (A, B, C) are selected, within distances not exceeding about one-half of the expected wavelength Λ of the perturbation. Site

B is taken to be the center of a topocentric reference frame whose axis x is directed east, and the axis y is directed north. The receivers in this frame of reference have the coordinates (x_A, y_A), (0,0), (x_C, y_C). Such a configuration of the GPS receivers represents the GPS-array with a minimum number of the required elements. In regions with a dense network of GPS sites, we can obtain a large variety of GPS-arrays of a different configuration enabling the acquired data to be checked for reliability; in this paper we have exploited this possibility.

The input data include series of slant TEC values $I_A(t)$, $I_B(t)$, $I(t)$, as well as corresponding series of elevation values $\theta_s(t)$ and the azimuth $\alpha_s(t)$ of the LOS. For determining SAW characteristics, continuous series of measurements of $I_A(t)$, $I_B(t)$, $I_C(t)$ are selected with a length of at least a one-hour interval which includes the time of a earthquake.

To eliminate spatio-temporal variations of the regular ionosphere, as well as trends introduced by orbital motion of the satellite, a procedure is used to remove the trend involving a preliminary smoothing of the initial series with the selected time window. This procedure is better suited to the detection of a single pulse signal (N-wave) than the frequently used band-pass filter (Li et al., 1994; Calais and Minster, 1995, 1996; Fitzgerald, 1997; Calais et al., 1998). A limitation of the band-pass filter is the oscillatory character of the response which prevets from reconstructing the form of the N-wave.

Elevation $\theta_s(t)$ and azimuth $\alpha_s(t)$ values of the LOS are used to determine the location of the subionospheric point, as well as to calculate the elevation θ of the wave vector K_t of the disturbance from the known azimuth α (see formula (3)).

The most reliable results from the determination of SAW parameters correspond to high values of elevations $\theta_s(t)$ of the LOS because sphericity effects become reasonably small. In addition, there is no need to convert the slant TEC $\Delta I(t)$ to a 'vertical' value. In this paper, all results were obtained for elevations $\theta_s(t)$ larger than 30°.

Since the distance between GPS-array elements (from several tens of kilometers to a few hundred kilometers) is much smaller than that to the GPS satellite (over 20000 km), the array geometry at the height of the ionosphere is identical to that on the ground.

Fig. 2a shows typical time dependencies of an slant TEC $I(t)$ at the GPS-array BSHM station near the area of the earthquake of August 17, 1999. (heavy curve), one day before and after the earthquake (thin lines). For the same days; panel b shows TEC variations $\Delta I(t)$ after removal of a linear trend and smoothing by averaging over a sliding window of 5-min. Variations in frequency Doppler shift $F(t)$, 'reduced' to the sounding signal frequency of 136 MHz, for three sites of the array (KATZ BSHM GILB) on August 17, 1999, are presented in panel c.

Fig. 2 shows that fast N-shaped oscillations, with a typical period of about 390 s, are distinguished among slow TEC variations. The oscillation amplitude (up to 0.12 $TECU$) is far in excess of the background TEC fluctuation intensity as seen on the days before and after the earthquake. Variations in frequency Doppler shift $F(t)$ for spatially separated sites (KATZ BSHM GILB) are well correlated but are shifted relative to each other by an amount well below the period, which permits the SAW propagation velocity to be unambiguously determined. The 30 s sampling rate of the GPS data is not quite sufficient for determining small shifts of such signals with an adequate accuracy for different sites of the array. Therefore, we used a parabolic approximation of the $F(t)$-oscillations in the neighborhood of minimum $F(t)$, which is quite acceptable when the signal/noise ratio is high.

Taking into account the good signal/noise ratio (better than 1), and knowing the coordinates of the array sites A, B and C, we determine the horizontal projection of the phase velocity V_h from time shifts t_p of a maximum deviation of the frequency Doppler shift $F(t)$. Preliminarily measured shifts are subjected to a linear transformation with the purpose of calculating shifts for sites spaced relative to the central site northward N and eastward E. This is followed by a calculation of the E- and

N-components of V_x and V_y, as well as the direction α in the range of angles 0–360° and the modulus V_h of the horizontal component of the SAW phase velocity

$$\begin{aligned} \alpha &= \arctan(V_y/V_x) \\ V_h &= |V_x V_y|(V_x^2 + V_y^2)^{-1/2} \end{aligned} \tag{5}$$

where V_y, V_x are the velocities with which the phase front crosses the axes x and y. The orientation α of the wave vector K, which is coincident with the propagation azimuth of the SAW phase front, is calculated unambiguously in the range 0–360° subject to the condition that $arctan(V_y/V_x)$ is calculated having regard to the sign of the numerator and denominator.

The above method for determining the SAW phase velocity neglects the correction for orbital motion of the satellite because the estimates of V_h obtained below exceed an order of magnitude as a minimum the velocity of the subionospheric point at the height of the ionosphere for elevations $\theta_s > 30°$ (Afraimovich et al., 1998).

Obviously the method presented above can be used if the distance between GPS stations is much shorter than the TEC disturbance wavelength Λ and the distance from the earthquake epicenter to the array. This corresponds to the detection condition in the far-field zone.

From the delay $\Delta t = t_p - t_0$ and the known path length between the earthquake focus and the subionospheric point we calculated also the SAW mean velocity V_a in order to compare our estimates of the SAW phase velocity with the usually used method of measuring this quantity.

3.2 Determination of the wave vector elevation θ and the velocity modulus V_t of the shock wave

Afraimovich et al. (1992) showed that for the Gaussian ionization distribution the TEC disturbance amplitude (M) is determined by the aspect angle γ between the vectors K_t and r, as well as by the ratio of the wavelength of the disturbance Λ to the half-thickness of the ionization maximum h_d

$$M \propto \exp\left(-\frac{\pi^2 h_d^2 \cos^2\gamma}{\Lambda^2 \cos^2\theta_s}\right). \quad (6)$$

In the case under consideration (see below), for a phase velocity on the order of 1 km/s and for a period of about 200 s, the wavelength Λ is comparable with the half-thickness of the ionization maximum h_d. When the elevations θ_s are 30°, 45°, 60° , the 'beam-width' $M(\gamma)$ at 0.5 level is, respectively, 25°, 22° and 15°. If h_d is twice as large as the wavelength, then the beam tapers to 14°, 10° and 8°, respectively.

The beam-width is sufficiently small that the aspect condition (3) restricts the number of beam trajectories to the satellite, for which it is possible to detect reliably the SAW response in the presence of noise (near the angles $\gamma = 90°$). On the other hand, formula (3) can be used to determine the elevation θ of the wave vector K_t of the shock wave at the known value of the azimuth α (Afraimovich et al., 1998). Hence the phase velocity modulus V_t can be defined as

$$V_t = V_h \cdot cos(\theta) \quad (7)$$

The above values of the width $M(\gamma)$ determine the error of calculation of the elevations θ (of order 20° to the above conditions).

3.3 Determining the position of the SAW source without regard for refraction corrections

The ionospheric region that is responsible for the main contribution to TEC variations lies in the neighborhood of the maximum of the ionospheric F-region, which does determine the height h_i of the penetration point. When selecting h_i, it should be taken into consideration that the decrease in electron density with height above the main maximum of the F_2-layer proceeds much slower than below this maximum. Since the density distribution with height is essentially a 'weight function' of the TEC response to a wave disturbance (Afraimovich et al., 1992), it is appropriate to use, as h_i, the value exceeding the true height of the layer $h_m F2$ maximum by

about 100 km. h_mF2 varies between 250 and 350 km depending on the time of day and on some geophysical factors which, when necessary, can be taken into account if additional experimental data and current ionospheric models are available. In all calculations that follow, $h_i = 400$ km is used.

To a first approximation, it can be assumed that the imaginary detector, which records the ionospheric SAW response in TEC variations is located at this altitude. The horizontal extent of the detection region, which can be inferred from the propagation velocity of the subionospheric point as a consequence of the orbital motion of the GPS satellite (on the order of 70 –150 m/s; see Pi at al., 1997), and from the SAW period (on the order of 200 s — see Section 4), does not exceed 20–40 km, which is far smaller than it 'vertical size' (on the order of the half-thickness of the ionization maximum h_d).

From the GPS data we can determine the coordinates X_s and Y_s of the subionospheric point in the horizontal plane $X0Y$ of a topocentric frame of reference centered on the point B(0,0) at the time of a maximum TEC deviation caused by the arrival of the SAW at this point. Since we know the angular coordinates θ and α of the wave vector K_t, it is possible to determine the location of the point at which this vector intersects the horizontal plane $X'0Y'$ at the height h_w of the assumed source. Assuming a rectilinear propagation of the SAW from the source to the subionospheric point and neglecting the Earth sphericity, the coordinates X_w and Y_w of the source in a topocentric frame of reference can be defined as

$$X_w = X_p - (h_i - h_w)\,\frac{\cos\theta\sin\alpha}{\sin\theta} \tag{8}$$

$$Y_w = Y_p - (h_i - h_w)\,\frac{\cos\theta\cos\alpha}{\sin\theta} \tag{9}$$

The coordinates X_w and Y_w, thus obtained, can readily be recalculated to the values of the latitude and longitude (ϕ_w and λ_w) of the source.

For SAW generated during earthquakes, industrial explosions and underground tests of nuclear devices, h_w is taken to be equal to 0 (the source lying at the ground level).

4 Results of measurements

Hence, using the transformations described in Section 3, we obtain the parameters set determined from TEC variations and characterizing the SAW (see Table 3).

Let us consider the results derived from analyzing the ionospheric effect of SAW during earthquake August 17, 1999 obtained at the array (KATZ, BSHM, GILB) for PRN 6 (at the left of Fig. 2, and line 2 in Table 3).

In this case the delay of the SAW response with respect to the time of the earthquake is 20 min (DAY 229). The SAW has the form of an N-wave with a period T of about 390 s and an amplitude $A_I = 0.12\ TECU$, which is an order of magnitude larger than TEC fluctuations for background days (DAY 228, DAY 230). It should be noted, however, that this time interval was characterized by a very low level of geomagnetic activity (-14 nT).

The amplitude of a maximum frequency Doppler shift A_F at the 'reduced' frequency of 136 MHz was found to be 0.04 Hz. In view of the fact that the shift F is inversely proportional to the sounding frequency squared (Davies, 1969), this corresponds to a Doppler shift at the working frequency of 13.6 MHz and the equivalent oblique-incidence sounding path of about $A_F = 4$ Hz.

Solid curves in Fig. 1a represent the trajectories of the subionospheric points for each GPS satellite at the height h_i=400 km during the time interval 0.0–0.8 UT for August 17, 1999, and 17.0–17.4 UT for November 12, 1999. Dark diamonds along the trajectories correspond to the coordinates of the subionospheric points at time t_p of a maximum deviation of the TEC (Fig. 2b and Fig. 2e). Crosses show the positions of the earthquake epicenters. Asterisks mark the source location at 0 km altitude inferred from the data from the GPS arrays. Numbers at the asterisks correspond to the respective day numbers. Straight dashed lines that connect the expected source and the subionospheric point represent the horizontal projection of the wave vector K_t.

The azimuth α and elevation θ of the wave vector K_t whose horizontal projection is shown in Fig. 1a by a dashed line and is marked by K_1, are 154° and 26°,

respectively. The horizontal component and the modulus of the phase velocity were found to be $V_h = 1307$ m/s and $V_t = 1174$ m/s. The source coordinates at 0 km altitude were determined as $\phi_w = 39.1^\circ$ and $\lambda_w = 25.9^\circ$. The alculated (by neglecting refraction corrections) location of the source roughly was close the earthquake epicenter.

The 'mean' velocity of about $V_a = 870$ m/s, determined in a usual manner from the response delay with respect to the start, was smaller then the phase velocity V_t. Conceivably this is associated with an added delay of the response as a consequence of the refraction distortions of the SAW path along the LOS which were neglected in this study.

Similar results for the array (KABR, TELA, GILB) and PRN 30 were also obtained for the earthquake of November 12, 1999. They correspond to the projection of the vector K_2 in Fig. 1a, the time dependencies in Fig. 2 at the right, and line 7 in Table 3. The only point deserving mention here is that the SAW amplitude was somewhat smaller than that for the earthquake of August 17, 1999. With an increased level of geomagnetic activity (-44 nT), this led to a smaller (compared with August 17, 1999) signal/noise ratio; yet this did not preclude reliable estimates of the SAW parameters.

A comparison of the data for both earthquakes showed a reasonably close agreement of SAW parameters irrespective of the level of geomagnetic disturbance, the season, and the local time.

To convince ourselves that the determination of the main parameters of the SAW form and dynamics is reliable for the earthquakes analyzed here, in the area of the earthquake we selected different combinations of three sites out of the sets of GPS stations available to us, and these data were processed with the same processing parameters. Relevant results (including the average results for the sets Σ), presented in Table 3 and in Fig. 1a (SAW source position), show that the values of SAW parameters are similar, which indicates a good stability of the data, irrespective of the GPS-array configuration.

The aspect condition (3), corresponding to a maximum amplitude of the TEC response to the transmission of SAWs, was satisfied quite well for this geometry, simultaneously for all stations. This is confirmed by a high degree of correlation of the SAW responses at the array elements (Fig. 2c and Fig. 2f), which made it possible to obtain different sets of triangles out of the six GPS stations available to us.

The relative position of the GPS stations was highly convenient for determining the SAW parameters during the earthquakes in Turkey, and met the implementation conditions for the method described in Section 3.1. Thus, the distance between stations (100-150 km at most) did not exceed the SAW wavelength of about 200-300 km, and was far less than the distance from the epicenter to the array (1000 km).

Let us consider the results derived from analyzing the ionospheric effect of SAW during earthquake January 13, 2001, obtained at the array (TEGU, MANA, ESTI) for PRN13 (at the left of Fig. 3 and line 11 in Table 3).

In this case the delay of the SAW response with respect to the time of the earthquake is 15 min (DAY 013). The SAW has the form of oscillations with a period T of about 270 s and an amplitude $A_I = 0.2\ TECU$, which is an order of magnitude larger than TEC fluctuations for background days (DAY 012, DAY 014). It should be noted, that this time interval was characterized by a very low level of geomagnetic activity (4 nT).

Similar results for the array (SAMP, NTUS, BAKO) and PRN 03 were also obtained for the earthquake of June 4, 2000. (at the right of Fig. 3 and line 10 in Table 3).

Note that in this case the response amplitude exceeded twice, as a minimum, that for the other events under consideration. It is not improbable that this is due to the maximum magnitude of the earthquake in Southern Sumatera (see Table 1).

Unfortunately, because of the inadequately well-developed network of stations, for the earthquakes in Southern Sumatera (June 4, 2000) and off the coast of Central America (January 13, 2001) for each of these events it was impossible to select arrays

meeting the applicability conditions of the method for determining the SAW wave vector parameters described in Section 3.1.

It is evident from the geometry in Fig.1b and Fig. 1c that the earthquake epicenters lay inside the GPS arrays, which does not meet the far-field zone condition. It is possible that this is also responsible for the form of the response (presence of strong oscillations) which differs from the N-form of the response for the earthquakes in Turkey. On this basis, for these earthquakes we can point out only the very fact of reliable detection of the response, and determine its amplitude A_I, typical period T, delay $\Delta t = t_p - t_0$, and velocity V_a (see Table 3). The values of these quantities were close to the data obtained for the earthquakes in Turkey.

5 Discussion

The data of Table 3 are quite sufficient to estimate the position of the disturbances under discussion in the diagnostic diagram of the atmospheric waves. Specifically, the values of the characteristic periods of bipolar signals, presented in Fig. 2b and Fig. 2e, are $T_1 \approx 300$ s, and $T_2 \approx 200$ s. The wave vectors are at the angles $\beta_1 \approx 70^\circ$ and $\beta_2 \approx 50^\circ$ with vertical. At the height $z \approx 400$ km, in turn, the periods, corresponding to local frequencies of the acoustic cut-off ω_a and the Brunt-Väisälä ω_b, are: $T_a = 2\pi/\omega_a \approx 950$ s, $T_b = 2\pi/\omega_b \approx 1050$ s.

In an isothermal atmosphere, only harmonics with periods larger than $T_b/sin\ \beta$ can be assigned to the branch of internal gravity waves. This value exceeds significantly the values of $T_{1,2}$. Furthermore, $T_{1,2}$ is considerably smaller than T_a. Hence we can contend that under conditions of the real (nonisothermal) atmosphere the disturbances under discussion almost entirely pertain to the branch of acoustic waves.

Since in (short period) acoustic waves the variation ΔN in neutral density N satisfies the relation $\Delta N/N \approx u/C$ (u is the gas velocity in the wave, and C is the local velocity of sound), it is possible to make a lower estimate of the intensity u/C of the waves at the expected altitudes $z_{eff} \approx 350$–400 km: $\Delta N/N \approx \Delta N_e/N_e \approx$

$\Delta I/I \approx 0.02-0.04$. In this estimation, the influence of the magnetic field is omitted, and the index e refers to electrons. The actual intensity of the acoustic wave must be higher than the estimated value presented above.

In the case of an earthquake, the movements of the terrestrial surface are plausible sources of acoustic waves. A generally known source of the first type is the Rayleigh surface wave propagating from the epicentral zone. The ground motion in the epicentral area is the source of the second type. Let us discuss these possibilities.

5.1 The Rayleigh wave

The phase propagation velocity of the Rayleigh wave $V_R \approx 3.3$ km/s. Since $V_R \gg C_0$, where $C_0 \approx 0.34$ km/s is the sound velocity at the ground, only acoustic waves can be emitted (Golitsyn and Klyatskin, 1967). At a sufficient distance from the epicenter where the curvature of the Rayleigh wave front can be neglected, and with the proviso that $\omega \gg \omega_a$, acoustic waves are emitted at the angle $\beta_R \approx arcsin(C_0/V_R) \approx 6^\circ$ to the vertical.

Rayleigh waves propagate generally in the form of a train consisting of several oscillations whose typical period only rarely exceeds several tens of seconds. Acoustic waves are emitted upward in the form of the same train. Because of a strong absorption of the periodic wave, the only thing that is left over in the case of the acoustic train at heights $z \geq 350$ km is the leading phase of compression. It seems likely that only in the case of strong earthquakes (Alaskian earthquake of 1964), even at large distances from the epicenter, the disturbance (the leading portion of the acoustic train) that remains from the acoustic train, can have at these altitudes a duration of about 100 s, and quite an appreciable ($u/C > 0.1$) intensity (Orlov and Uralov, 1987) the nonlinear acoustics approximation.

Unfortunately, the parameters of Rayleigh waves in the neighborhood of the subionospheric points appearing in Table 3 are unknown to us. However, a most pronounced bipolar character of the main signal (Fig. 2b, Fig. 2e, Fig. 3b and Fig. 3e), its intensity, and its long duration cast some doubt upon the fact that it is the

Rayleigh wave which is responsible for its origin. Such a conclusion is consistent with the observed propagation direction of the bipolar pulse, which makes a large angle with the vertical: $\beta_{1,2} \approx 70$–$50^\circ \gg \beta_R^{"} \approx 15$–$18^\circ$.

Here it is taken into consideration that the acoustic ray originating from a point on the ground at the angle of $\beta_R \approx 6^\circ$ now makes at the heights $z = z_{eff}$ an angle $\beta_R^{"} > \beta_R$ because of the refraction effect in a standard atmospheric model: $C_0/sin\ \beta_R = C/sin\ \beta_R^{"} = const = V_R$, $C(z = z_{eff}) \approx 0.9$–$1$ km/s.

The presence of strong winds at ionospheric heights can alter the value of β_R. However, irrespective of the atmospheric model, the phase velocity V_h (Table 3) of the horizontal trace of the acoustic disturbance generated by the Rayleigh wave must coincide with V_R, and this is also not observed: $V_h \ll V_R$.

5.2 The epicentral emitter

The detection of ionospheric disturbances, which are presumably generated by a vertical displacement of the terrestrial surface directly in the epicentral zone of an earthquake, using the GPS probing method, is reported in (Calais and Minster, 1995).

Results of the present study lend support to the above conjecture. However, the specific formation mechanism for the disturbance itself is still unclear. An approach to solving this problem is contained in earlier work, and involves substituting the epicentral emitter for a surface velocity point source or an explosion. In particular, the substitution of the earthquake zone for a point source turns out to be fruitful when describing long-period internal gravity waves at a very long (thousands of kilometers) distance from the epicenter (Row, 1967). The visual resemblance of ionospheric disturbances at short (hundreds of kilometers) distances from the earthquake epicenter to disturbances from surface explosions is discussed in (Calais et al., 1998).

It should be noted that ionospheric disturbances generated by industrial surface and underground nuclear explosions are also visually similar. However, the genera-

tion mechanisms for disturbances are fundamentally different in this case (Rudenko and Uralov, 1995). The radiation source in underground nuclear tests is, as in the case of earthquakes, the terrestrial surface disturbed by the explosion. The intensity and spectral composition of the generated acoustic signal reveal a strong (unlike the surface explosion) dependence on the zenith angle, and are wholly determined by the form, size and characteristics of the movement of the terrestrial surface in the epicentral zone of the underground explosion.

In this Section, we shall propose a model which, we hope, will help to understand the generation mechanism for acoustic disturbances — the subject of this paper. Because of the complexity of the problem formulated, and for lack of sufficient data on characteristics of the movement of the terrestrial surface in epicentral zones of earthquakes, the idealized model under discussion has an illustrative character. The computational scheme proposed below represents a simplified variant of the scheme used in Rudenko and Uralov, (1995) to calculate ionospheric disturbances generated by an underground confined nuclear explosion.

5.3 The problem of radiation of the acoustic signal

For the sake of simplicity, we consider a problem having an axial symmetry about the vertical axis z passing through the earthquake epicenter $r = z = 0$. The epicentral emitter is a set of plane annular velocity sources with the specified law of motion along the vertical $U(r,t)$. Since our interest is with the estimation of the characteristics of an acoustic disturbance at a sufficient distance from the emitter, we take advantage of the far-field approximation of a linear problem of radiation. In the approximation of linear acoustics $\omega \gg \omega_a$ and with no absorption present, the gas velocity profile in the wave can be estimated by the expression:

$$u(\tau,\beta) = \frac{A}{\pi R C_0} \int_0^L \int_{-\infty}^{+\infty} \frac{a(t^{'},r) r dr dt^{'}}{\sqrt{y^2 - (\tau - t^{'})^2}|_{|\tau - t^{'}| \le y}} \tag{10}$$

where $\tau = t - \int_0^l dl/C$, $y = \frac{r sin\beta}{C_0}$. Here β is the zenith angle of departure of the acoustic ray from the point $r = z = 0$. l is the group path length (the distance

along the ray). $a(t^{'},r) = \frac{dU(r,t)}{dt}$ is the vertical acceleration of the terrestrial surface. $A = A(z) = \sqrt{\frac{C_0\rho_0}{C\rho}}$ is the acoustic factor. $\rho_0,\ \rho$ stand for the air density at the ground and at the height z, respectively, and L is a typical radius of the epicentral emitter.

In an isothermal atmosphere where the ray trajectories are straight lines, the quantity $R = (\sqrt{r^2 + z^2} = l)$ is the radius of a divergent (in the far-field approximation) spherical wave. In this case the cross-section of the selected ray tube $S \propto R^2$. In the real atmosphere the value of S is determined from geometrical optics equations, and using the expression (10) requires a further complication of the computational scheme. Nevertheless, to make estimates we shall use only the relation (10), and, in doing so, the value of R will be corrected.

The case $\beta = 0$ (and also $l = R = z$) is a special one:

$$u(\tau, \beta = 0) = \frac{A}{RC_0}\int_0^L a(\tau, r)rdr \tag{11}$$

Let us discuss the situation where all ring-type emitters 'operate' synchronously: $U(r,t) = U(t)$. In this case the epicentral zone is emitting as a round piston $2L$ in diameter. Assume also that with a shock of the earthquake, the vertical displacement ξ, the velocity $U = d\xi/dt$ and the acceleration $a = dU/dt$ are time dependent, as shown in Fig. 4a. For a rectangular velocity impulse, i.e. in the limit $\Delta t \gg \delta t \to 0$ (in this case $a\delta t \to \pm U_0\delta(t^{'})$, where $\delta(t^{'})$ is a delta-function), from (10) we can obtain

$$u(\tau, \beta) = \frac{U_0C_0A}{\pi R sin^2\beta}\{\sqrt{y_L^2 - \tau^2}|_{|\tau|\le y_L} - \sqrt{y_L^2 - (\tau - \Delta t)^2}|_{|\tau - \Delta t|\le y_L}\} \tag{12}$$

where $y_L = \frac{Lsin\beta}{C_0}$; $U_0,\ \Delta t$ are the amplitude and duration of the rectangular velocity impulse. In this case the vertical displacement of the terrestrial surface after the earthquake shock is $\xi_0 = U_0\Delta t$. In the strict sense, the expression (12) holds true if the condition $y_L \gg \delta t$ is satisfied, i.e. with zenith angles $\beta \gg \beta^* \approx arcsin\frac{C_0\delta t}{L}$. Here δt is the operation duration of the terrestrial shock at the beginning of the movement and at the stop of the piston. When $\beta \approx \beta^* \ll 1$, the expression (12) and

the expression (11), in view of $\delta t \neq 0$, yield approximately identical signals. What actually happens is that the validity of the expression (12) will break down still earlier, and we are justified in using it only for zenith angles $\beta > \beta^{**} = arctan(\frac{L}{z}) > \beta^{*}$.

The curves in Fig. 4b give an idea of the relative amplitude and form of acoustic signals $u(\tau, \beta)$ in the far-field zone of radiation of the piston $2L = 60$ km in diameter. The duration of the rectangular velocity impulse of the piston was chosen arbitrarily, $\Delta t = 10$ s. The signals correspond to the expression (12) under the assumption of a homogeneous, $A = 1$, $C = C_0 \approx 0.34$ km/s, atmosphere. The zenith angles are $\beta = 10^{\circ}, 20^{\circ}, 40^{\circ}, 60^{\circ}, 90^{\circ}$. The spherical surface $R = const$ serves as a reference. The abscissa axis indicates the time τ in seconds, and the axis of ordinates indicates the gas velocity u. In this case the amplitude of the most intense signal ($\beta = 10^{\circ}$) is taken to be unity.

With increasing β, the amplitude of the signals u_{max} decreases, and the duration T increases. The leading and trailing edges of the bipolar pulses in Fig. 2 and Fig. 3 have an equal duration Δt. The positive part of the bipolar pulse corresponds to the compression phase of the acoustic wave, and the negative part refers to the rarefaction phase. The area of the compression phase (in coordinates u, t) equals the largest displacement χ_{+} of a unit volume of the atmosphere in the direction of propagation (along the ray) of the wave. A total area of a bipolar pulse is zero: $\chi_{+} = -\chi_{-}$. For acoustic signals, described by the expression (12), the following useful relations hold true:

$$u_{max} = U_0 \frac{2AL}{\pi R sin\beta} \sqrt{\eta - \eta^2}; \quad T = 2y_L + \Delta t \tag{13}$$

$$\chi_{+} = \xi_0 \frac{AL}{2\pi R sin\beta} \{\sqrt{1 - \eta^2} + \frac{1}{\eta} arcsin\ \eta\}; \quad \eta = \frac{\Delta t}{2y_L} \tag{14}$$

5.4 The problem of acoustic signal propagation

The wave vectors K_t of the bipolar pulses make with the vertical the angles $\beta_1 = 70°$ and $\beta_2 = 50°$. With the adopted values of $z_{eff} = 350$–400 km, the distances of the corresponding subionospheric points from the earthquake epicenters in Fig. 1a are approximately $r_1 = 800$ km and $r_2 = 600$ km. The rays, constructed in the approximation of linear geometrical acoustics (LGA) and having at the heights $z = z_{eff}$ ($C(z = z_{eff}) \approx 0.9$–$1$ km/s) the propagation angles β_1 and β_2, correspond to the zenith angle of departure $\beta \approx 19$–$21°$ and $\beta \approx 15$–$17°$ at the level $z = 0$.

The fact that these values of β satisfy the inequality $\beta \leq \beta^* \approx 25$–$30°$, is in reasonably good agreement with the familiar picture of rays from a ground-level point source — the rays with $\beta \geq \beta^*$ are captured by the atmospheric waveguide $z \leq z^* = 120$ km, and only the rays emitted upward inside the solid angle $\Omega^* \approx 1$ sterad can penetrate to the heights $z > z^*$. In standard models of the atmosphere, however, to the values of the angles $\beta_{1,2}(z = z_{eff})$ there correspond the locations of subionospheric points lying several hundreds kilometers nearer to the epicenter compared with the experimental values of $r_1 \approx 800$ km and $r_2 \approx 600$ km. This inconsistency can be due to two reasons.

One reason is that the value of $z_{eff} \approx 350$–400 km, which we are using, is too low. This is supported by the detection of velocities $V_t \approx 1.2$ km/s of traveling disturbances (Table 3) which exceed markedly the sound velocity $C \approx 0.9$–1 km/s at the heights of ≈ 350–400 km. However, it seems likely that such a discrepancy may be disregarded, in view of the errors of the measurement technique used (the probability of an additional heating of the upper atmosphere prior to the earthquake cannot be ruled out, however).

The increase of the actual value of z_{eff} can also be associated with a strong dependence (see (13), (14) and Fig. 4b) of the power of the emitted signal on the zenith angle of departure of the ray from the earthquake epicenter. Verifying this factor requires a more detailed analysis, based on particular data on vertical movements of the terrestrial surface in the epicentral zone. Such data are unavailable to us. Below

is a discussion only of the second reason for the above-mentioned inconsistency as a highly probable one.

The second reason may be associated with the violation of the validity conditions of the LGA approximation at a sufficient distance from the source of the acoustic disturbances under discussion. Indeed, the utilization of this approximation is justified until the parameters of the medium and of the wave itself change substantially on the size of the first Fresnel zone $d_F \approx \sqrt{\lambda l}$ that determines the physical (transverse) size of the ray. Typical wavelengths of the bipolar pulses under discussion at the heights $z = z_{eff}$ are large: $\lambda \approx 300$–200 km. Distance l along the expected ray is of order 900–700 km. Then $d_F \approx 520$–370 km, which exceeds substantially the scales of variation of atmospheric parameters. The value of d_F is actually somewhat smaller, because the typical scale of a disturbance decreases as it approaches the source. A violation of the LGA approximation at the above-mentioned distances from the epicentral source occurs also for model signals $\beta \geq 20^\circ$, shown in Fig. 4b.

The increasing violation of the applicability conditions of the LGA approximation with an increase of l implies the transport of the wave energy not strictly along the calculated rays but along the lines with a smaller curvature. With a mere estimate of the dilution factor R in the expressions (12), (13) and (14), in mind, these lines will be assumed to be straight when $z > z^*$ and to originate from an imaginary source lying at the height $z^* \approx 120$ km above the earthquake epicenter. Such a situation is also clearly manifested in the LGA approximation. At the heights $z > z^*$, at $t \approx 600$ s, for example, the surface of the wave front from the ground-level impulsive source resembles the surface of a hemisphere centered on the point $r \approx 0$, $z \approx z^*$.

Ultimately the energy that arrives from below inside the solid angle $\Omega^* \approx 1$ is scattered into a solid angle $\Omega \approx 2\pi$. From the condition of conservation of wave energy, it is possible to find $R_{1,2} = \sqrt{\frac{\Omega}{\Omega^*}}\sqrt{(\Delta z)^2 + r_{1,2}^2}$, when $\Delta z = z_{eff} - z^*$. When using the expressions (13), (14) in the subsequent discussion, we will take the quantity R_1 rather than R, and the value of the zenith angle of departure will be taken to be $\beta = 20^\circ$. These parameters approximately correspond to the generation

and propagation conditions of the signal from the first earthquake. The typical size of the epicentral zone of this earthquake was about $2L = 60$ km (according to the USGS data: www.neic.cr.usgs.gov). This same value of L was used in calculating the signals shown in Fig. 4b.

As is evident even from Fig. 4b (thick line), the duration of the signal, having a zenith angle of departure $\beta = 20°$, is about 70 s. When the signal propagates in the approximation of linear acoustics and with no absorption, its form and duration remain unchanging, and only its amplitude changes.

In actual conditions the combined effect of the nonlinear attenuation and linear absorption factors leads to a stretching of the bipolar pulse, and to a change of its form (we do not discuss the dispersion factor). In this case the effect of the nonlinearly factor occurs in such a manner that the integral value of χ_+, (14), calculated as an approximation of linear acoustics, remains as such in the approximation of nonlinear acoustic as well. Moreover, taking into account the finite width ΔT_{sh} of the shock front does not change this situation until $\Delta T_{sh} < T/4$. The linear absorption factor, in turn, somewhat reduces the true value of χ_+ because of the mutual diffusion of the compression and rarefaction phases. Nevertheless, for a hypothetical estimation of the earthquake parameters, we shall use the assumption about the conservation of the value of χ_+.

As is intimated by Table 3, the mean value of the TEC disturbance amplitude after the first earthquake is $A_I \approx 0.14\ TECU$ at the equilibrium value of $I \approx 5\ TECU$. Assuming that on the order of magnitude $A_I/I \approx u/C$ for a maximum gas velocity in the wave, we have an estimate of $u^{exp} \approx 30$ m/s. For the sinusoidal form of the bipolar pulse with a duration $T^{exp} \approx 350$ s, we find the experimental value of gas displacement along the direction of wave propagation: ${\chi_+}^{exp} = u^{exp}T^{exp}/\pi \approx 3$ km. Using the relation ${\chi_+}^{exp} \approx \chi_+$ it is possible to estimate the vertical displacement ξ_0 of the terrestrial surface in the epicentral zone of the earthquake. For this purpose, it seems reasonable to introduce the assumption about a short velocity impulse which models the main earthquake shock, $\eta \ll 1$, although the numerical value of χ_+ is

virtually independent of the value of η (14). In view of the above considerations, we then obtain:

$$\xi_0 \approx {\chi_+}^{exp} \pi R_1 sin\beta/(AL). \tag{15}$$

The uncertainty in the determination of ξ_0 is caused both by the uncertainty of the true values of the quantities involved in this relation and by the limitations of the acoustic signal generation model itself. In this case, of the greatest importance is the dependence of ξ_0 on the value of the acoustic parameter A, containing the atmospheric density ρ at the effective height $z = z_{eff}$ which we have introduced artificially. The employment of the MSISE90 atmospheric model (Hedin, 1991), calculated for the location and time of the first earthquake, gives the values of $\xi_0 \approx 60, 40$ and 25 cm, with the values of $z_{eff} = 350, 400$ and 450 km, respectively. In all cases it was assumed that $R_1 \approx 850\sqrt{2\pi}$ km, $\beta = 20°$, $L = 30$ km. The possibility of a vertical displacement of the terrestrial surface in the epicentral zone by several tens of centimeters seems real. In particular, (Calais and Minster, 1995) give the value of $\xi_0 \approx 40$ cm at the epicenter of the Mw=6.7 Northridge earthquake (California, 1994).

In view of the demonstration character of the above calculation, we have intentionally excluded from consideration the effects associated with the inclination of the magnetic field lines, and with the possible presence of strong winds at ionospheric heights. The presence of a magnetic field modifies the picture of transfer of movements from the neutral gas to the electron component of the ionosphere. Since the magnetic field is not entrained by the neutral gas, the field lines can be considered fixed. In this case the acceptable approximation would be the one, in which the electron component travels only along magnetic field lines with the velocity $u \cdot cos\psi$, where ψ is the angle between the magnetic field vector and the velocity vector of the neutral gas. Therefore, the quantity $u \cdot cos\psi$ must be involved in lieu of the quantity u in the expression $A_I/I \approx u/C$ that was used above.

Let us estimate the value of ψ for Turkey earthquakes. In the examples under discussion (Table 3), the horizontal projection K of the full wave vector K_t is virtually collinear to the horizontal component of the magnetic field. The wave vectors K_t, in turn, make with the vertical the angles from $\beta_1 \approx 70^\circ$ to $\beta_2 \approx 50^\circ$.

Since the magnetic dip in the middle of Turkey is about 60° (the angle is measured from the horizontal plane), $\psi \cong 20^\circ$–40°, and the value of $cos\psi \approx 0.94$–0.77 differs little from 1. It should be remembered, however, that taking into account this factor can be very important in the analysis of the complete picture of TEC disturbances above the earthquake or explosion source (see, for example, Calais et al., 1998).

The presence of the zonal and meridional winds at ionospheric heights leads to a displacement and deformation of the wave front, and hence give rise to a dependence of the acoustic wave intensity on the propagation direction. The decisive role in this case is played by the wind velocity gradient. This factor can be taken into account within the framework of the ray theory. However, a corresponding model calculation would be worthwhile in the analysis of experimental data obtained for a set of subionospheric points surrounding the acoustic wave source. In the present situation, however, where the number of subionospheric points used in the analysis is too small, and the uncertainty of the parameters of the acoustic emitter itself is too large, the solution of such an unwieldy problem would be an overrun of the accuracy which is pursued by the above computational scheme.

As follows from the expressions (13), maximum values of displacements and of the velocity of the neutral atmospheric species are attained directly above the earthquake epicenter. The signal duration is minimal, and does not seem to exceed a few tens of seconds at ionospheric heights. Since the wave vector of the disturbance is directed predominantly upward, the method of oblique-incidence ionospheric sounding in this case is a technique of choice for determining the waveform.

6 Conclusion

In this paper we have investigated the form and dynamics of shock-acoustic waves generated during earthquakes. We have developed a method of determining the SAW parameters using GPS arrays whose elements can be chosen out of a large set of the global network GPS stations. Unlike existing radio techniques, the proposed method estimates the SAW parameters without a priori information about the location and time of the earthquake. The implementation of the method is illustrated by an analysis of ionospheric effects of the earthquakes in Turkey (August 17, and November 12, 1999), in Southern Sumatera (June 4, 2000), and off the coast of Central America (January 13, 2001).

It was found that, in spite of the difference of the earthquake characteristics, the local time, the season, and the level of geomagnetic disturbance, for four earthquakes the time period of the ionospheric response is 180-390 s, and the amplitude exceeds by a factor of two as a minimum the standard deviation of background fluctuations in total electron content in this range of periods under quiet and moderate geomagnetic conditions.

As has been pointed out in the Introduction, some investigators report markedly differing values of the SAW propagation velocity — by as much as several thousands m/s, which is beyond the values of the sound velocity at the SAW propagation heights in the atmosphere. The method proposed in this paper opens up a possibility of determining the angular characteristics of the wave vector K_t and, accordingly, of estimating V_t. According to our data (Table 3), the elevation of the SAW wave vector varied within 20–44° , and the phase velocity of the SAW varied from 1100 to 1300 m/s. We determine the phase velocity of the equal TEC line at the height of the ionospheric F-region maximum which makes the main contribution to variations of the TEC between the receiver and the GPS satellite, and corresponds to the region of maximum sensitivity of the method. Since V_t approaches the sound velocity at these heights (Li et al., 1994) this makes it possible to identify the sound origin of the

TEC disturbance. The SAW source location, calculated without taking into account the refraction corrections, approximately corresponds to the earthquake epicenter.

7 Acknowledgements

We are indebted to G. M. Kuznetsova and A. V. Tashchilin for their calculation of the atmospheric parameters at the time of the earthquakes, as well as to E. A. Ponomarev, V. V. Evstafiev, P. M. Nagorsky, N. N. Klimov, and A. D. Kalikhman for their interest in this study, many pieces of useful advice, and active participation in discussions. Thanks are also due to V. G. Mikhalkosky for his assistance in preparing the English version of the manuscript. Finally, the authors wish to thank the referees for valuable suggestions which greatly improved the presentation of this paper. This work was done with support from both the Russian foundation for Basic Research (grant 99-05-64753) and RFBR grant of leading scientific schools of the Russian Federation No. 00-15-98509.

References

[1] **Afraimovich, E.L., Varshavsky, I.I., Vugmeister, B.O., et al.**, Influence of surface industrial explosions on Doppler and angular characteristics of the ionosphere-reflected radio signal, *Geomagnetizm i aeronomiya*, **24**, 322–324, 1984.

[2] **Afraimovich, E.L., Terechov, A.I., Udodov, M.Yu. and Fridman, S.V.**, Refraction distortions of transionospheric radio signals caused by changes in a regular ionosphere and by travelling ionospheric disturbances, *J. Atmos. Terr. Phys.*, **54**, 1013–1020, 1992.

[3] **Afraimovich, E.L., Palamartchouk, K.S. and Perevalova, N.P.**, GPS radio interferometry of travelling ionospheric disturbances, *J. Atmos. Terr. Phys.*, **60**, 1205–1223, 1998.

[4] **Blanc, E. and Jacobson, A.R.**, Observation of ionospheric disturbances following a 5-kt chemical explosion. 2. Prolonged anomalies and stratifications in the lower thermosphere after shock passage, *Radio Sci.*, **24**, 739–746, 1989.

[5] **Calais, E. and Minster, J.B.**, GPS detection of ionospheric perturbations following the January 1994, Northridge earthquake, *Geoph. Res. Lett.*, **22**, 1045–1048, 1995.

[6] **Calais, E. and Minster, J.B.**, GPS detection of ionospheric perturbations following a Space Shuttle ascent, Geoph. *Res. Lett.*, **23**, 1897–1900, 1996.

[7] **Calais, E., Minster, J.B., Hofton, M.A. and Hedlin, M.A.H.**, Ionospheric signature of surface mine blasts from Global Positioning System measurements, *Geoph. J. Int.*, **132**, 191–202, 1998.

[8] **Davies, K.**, *Ionospheric radio waves*. Blaisdell Publishing Company. A Division of Ginn and Company, Waltham, Massachusetts-Toronto-London, 1969.

[9] **Fitzgerald, T.J.**, Observations of total electron content perturbations on GPS signals caused by a ground level explosion, *J. Atmos. Terr. Phys.*, **59**, 829–834, 1997.

[10] **Golitsyn G.S. and Klyatskin, V.I.**, Vibrations in the atmosphere caused by movements of the terrestrial surface, *Izv. Akademii nauk SSSR, Fizika atmosfery I okeana*, **111**, 1044-1052, 1967.

[11] **Hedin, A.E.**, Extension of the MSIS thermosphere model into the middle and lower atmosphere, *J. Geophys. Res.*, **96**, 1152-1172, 1991.

[12] **Jacobson, A.R., and Carlos, R.C.**, Observations of acoustic–gravity waves in the thermosphere following Space Shuttle ascents, *J. Atmos. Terr. Phys.*, **56**, 525–528, 1994.

[13] **Li, Y.Q., Jacobson, A.R., Carlos, R.C., Massey, R.S., Taranenko, Y.N. and Wu, G.**, The blast wave of the Shuttle plume at ionospheric heights, *Geoph. Res. Lett.*, **21**, 2737–2740, 1994.

[14] **Mercier, C. and Jacobson, A.R.**, Observations of atmospheric gravity waves by radio interferometry: are results biased by the observational technique, *Annales Geophysicae*, **15**, 430–442, 1997.

[15] **Nagorsky, P.M.**, The inhomogeneous structure of the ionospheric F-region produced by rockets, *Geomagnetizm i aeronomiya*, **38**, 100–106, 1998.

[16] **Orlov, V.V. and Uralov, A.M.**, Atmospheric response to the Rayleigh wave generated by an earthquake, In: *Issledovaniya po geomagnetismu, aeronomii i fizike Solntsa*, Moscow: Nauka, **78**, 28-40, 1987.

[17] **Pi, X., Mannucci, A.J., Lindgwister, U.J. and Ho, C.M.**, Monitoring of global ionospheric irregularities using the woldwide GPS network, *Geophys. Res. Lett.*, **24**, 2283–2286, 1997.

[18] **Row, R.V.**, Acoustic-gravity waves in the upper atmosphere due to a nuclear detonation and an earthquake, *J. Geophys. Res.*, **72**, 1599-1610, 1967.

[19] **Rudenko, G.V., Uralov, A.M.**, Calculation of ionospheric effects due to acoustic radiation from an undeground nuclear explosion, *J. Atmos. Terr. Phys.*, **57**, 225-236, 1995.

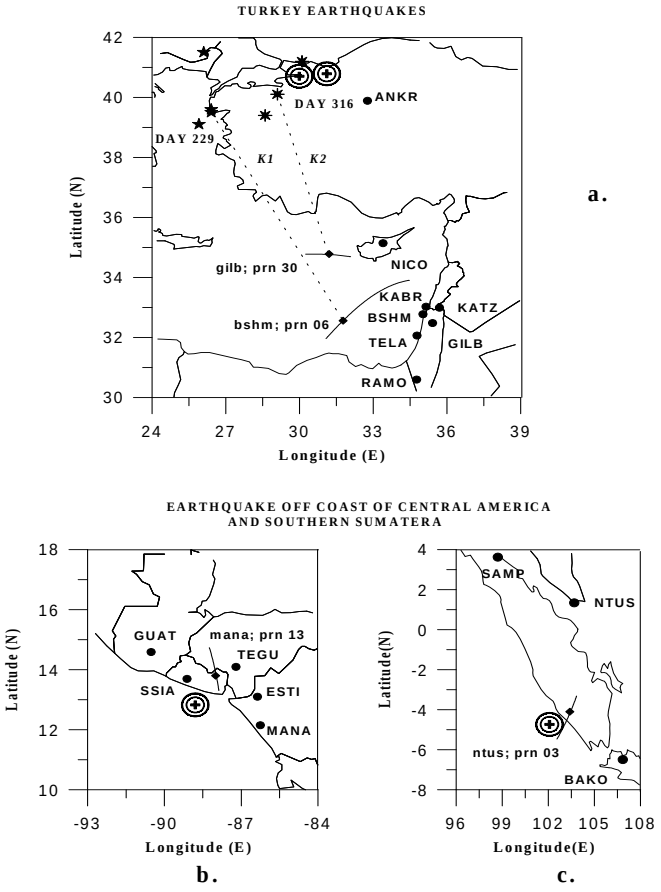

Fig. 1: Experimental geometry during the earthquakes in Turkey – a). Crosses show the positions of the earthquake epicenters. Solid curves represent the trajectories of the subionospheric points for each GPS satellite at the height h_i=400 km. Dark diamonds along the trajectories correspond to the coordinates of the subionospheric points at time t_p of a maximum deviation of the TEC. Heavy dots and large lettering show the location and the names of the GPS stations, while lower-case letters along the trajectories refer to station names and PRN numbers of the GPS satellites for these trajectories.

Asterisks mark the source location at 0 km altitude inferred from the data from the GPS arrays. Numbers at the asterisks correspond to the respective day numbers. Straight dashed lines that connect the expected source and the subionospheric point represent the horizontal projection of the wave vector $\boldsymbol{K}_t$. The scaling of the coordinate axes is chosen from considerations of an approximate equality of the linear dimensions along the latitude and longitude.

The same, but for the earthquakes off the coast of Central America on January 13, 2001 – b), and in Southern Sumatera on June 4, 2000– c).

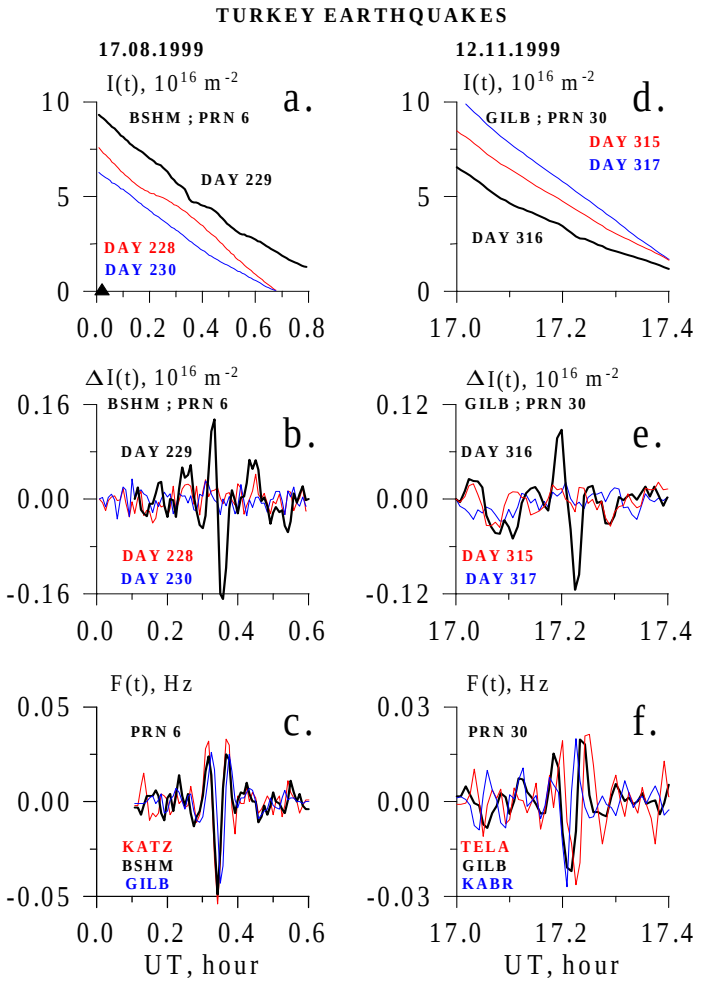

Fig. 2: Time dependencies of slant TEC $I(t)$ at one of the three sites of the GPS-array in the area of the earthquakes on August 17 and November 12, 1999, on the day of earthquake (heavy curve), and one day before and one day after the event (thin curves) — panels a, d. Panels b, e — for the same days but the TEC variations $\Delta I(t)$ with the linear trend removed and with a smoothing with a time window of 5 min; panels c, f — variations of the frequency Doppler shift $F(t)$ 'reduced' to the sounding signal frequency of 136 MHz, for three sites of the arrays, days of earthquake. All panels show day numbers, GPS station names, and PRN numbers of the GPS satellites.

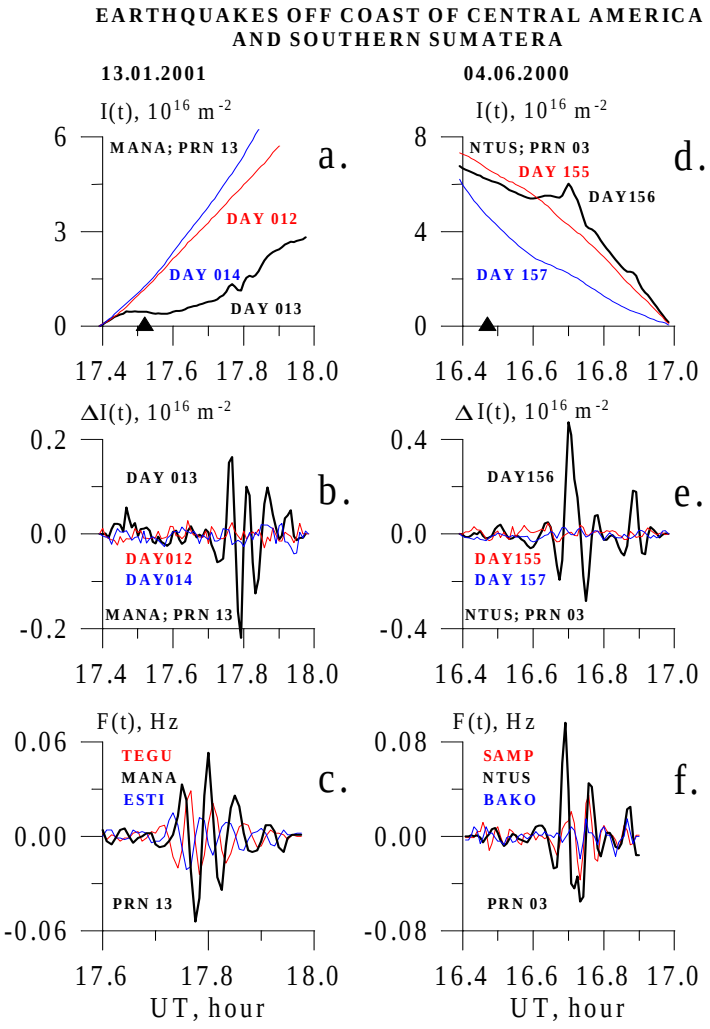

Fig. 3: Same as in Fig.2, but for the earthquakes off the coast of Central America, January 13, 2001 – at the left, and in Southern Sumatera, June 4, 2000 – at the right.

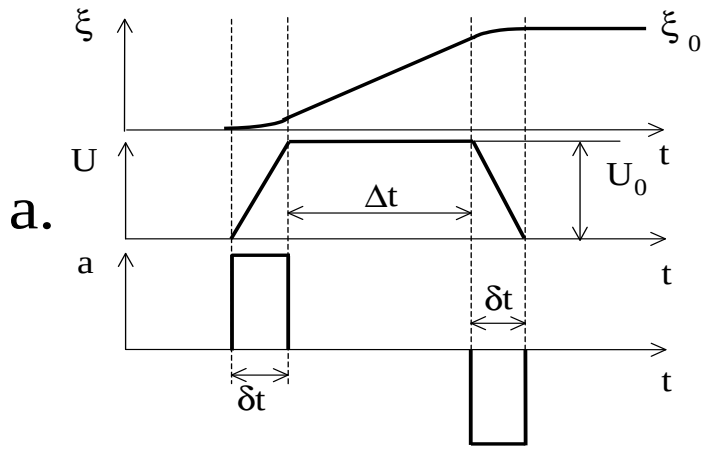

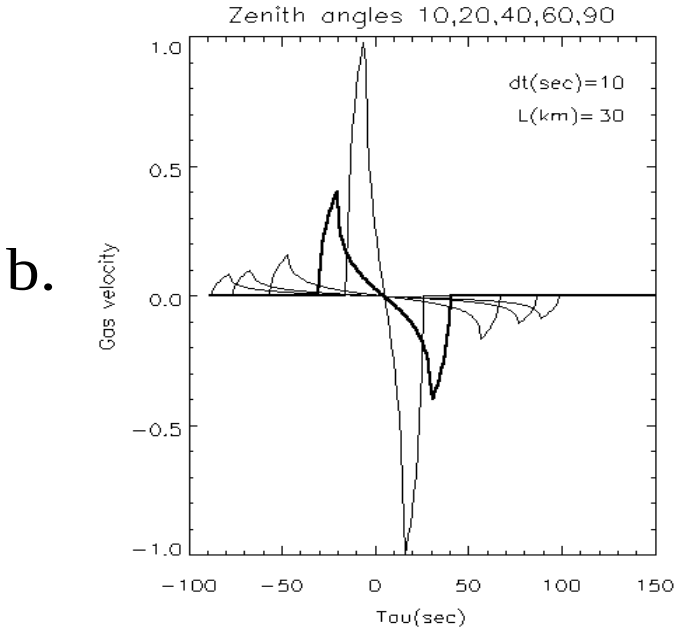

Fig. 4: a. Model time dependence (from top to bottom) of the vertical displacement ξ, the velocity $U = d\xi/dt$ and the acceleration $a = dU/dt$ of the terrestrial surface in the epicentral zone of the earthquake.

b. Acoustic signals $u(\tau, \beta)$ in the far-field radiation zone of the piston $2L = 60$ km in diameter. The piston's velocity has the form of a rectangular impulse of a duration $\Delta t = 10$ s. The signals correspond to the expression (12) under the assumption of a homogeneous atmosphere; $A = 1$, and $C = C_0 \approx 0.34$ km/s. The zenith angles are $\beta = 10°, 20°, 40°, 60°$, and $90°$. The abscissa axis indicates the time τ in seconds, and the axis of ordinates indicates the gas velocity u. The amplitude of the strongest signal $\beta = 10°$ is taken to be unity.

Table 1: General information about earthquakes

N	Epicenter	Data	t_0 (UT)	Depth (km)	Magnitude mb Ms Mw	DST (nT)
1	40.70 N, 29.99 E	Aug. 17 1999 (DAY 229)	00:01:39	17	6.3 7.8 7.4	-14
2	40.79 N, 31.11 E	Nov. 12 1999 (DAY 316)	16:57:20	10	6.5 7.5 7.1	-44
3	4.72 S, 102.1 E	Jun. 4 2000 (DAY 156)	16:28:26	33	6.8 8.0 7.7	+8
4	12.83 N, 88.79 W	Jan. 13 2001 (DAY 013)	17:33:29	39	- - 7.6	+4

Table 2: General information about earthquakes

N	Sites	Geograph. latitude	Geograph. longitude	N	Sites	Geograph. latitude	Geograph. longitude
1	ANKR	39.887	32.759	9	TEGU	14.090	-87.206
2	BSHM	32.778	35.022	10	SSIA	13.697	-89.117
3	GILB	32.479	35.416	11	MANA	12.149	-86.2489
4	KABR	33.022	35.145	12	GUAT	14.590	-90.520
5	KATZ	32.995	35.688	13	ESTI	13.100	-86.3621
6	NICO	35.141	33.396	14	SAMP	3.622	98.715
7	RAMO	30.597	34.763	15	NTUS	1.346	103.680
8	TELA	32.067	34.780	16	BAKO	-6.491	106.849

Table 3: The parameters of shock-acoustic waves

No.	Sites	t_p (UT)	Δt, sec.	T, sec.	A_I, TECU	A_F, Hz	$\theta,^\circ$	$\alpha,^\circ$	V_h, m/s	V_t, m/s	V_α, m/s	$\varphi_w,^\circ$ $\lambda_w,^\circ$
1999 Aug. 17; t_0=00:01:39 UT												
1	KABR	00:21:04	1165	360	0.15	0.037	24.9	155	1296	1174	873	39.6
	BSHM	00:21:19	1180	300	0.14	0.049					862	26.4
	KATZ											
2	GILB	00:21:54	1215	390	0.12	0.043	26.1	154	1307	1174	868	39.1
	KATZ											25.9
	BSHM											
3	KATZ	00:21:23	1184	360	0.19	0.05	25.1	155	1303	1179	854	39.5
	KABR											26.4
	GILB											
4	TELA	00:22:14	1235	360	0.1	0.026	19.9	161	1238	1164	894	41.5
	BSHM											26.1
	GILB											
5	$\sum$			354	0.14	0.04	24.1	156	1286	1173	870	39.9
												26.2
1999 Nov. 12; t_0=16:57:20 UT												
6	KABR	17:12:58	938	180	0.06	0.027	29.5	194	1285	1119	807	42.2
	BSHM	17:13:21	961	180	0.07	0.021					787	30.1
	GILB											
7	TELA	17:14:09	1009	210	0.097	0.021	43.8	180	1487	1073	838	39.4
	KABR											28.6
	GILB											
8	GILB	17:13:39	979	210	0.09	0.022	39.6	184	1663	1280	817	40.1
	BSHM											29.1
	TELA											
9	$\sum$			195	0.079	0.023	37.6	186	1478	1157	812	40.5
												29.2
2000 Jun. 4; t_0=16:28:26 UT												
10	SAMP	16:46:12	1092	270	0.1	0.04					558	
	NTUS	16:42:16	856	270	0.5	0.09					503	
	BAKO	16:49:16	1276	240	0.06	0.02					642	
2001 Jan. 13; t_0=17:33:29 UT												
11	TEGU	17:45:11	851	240	0.09	0.03					591	
	ESTI	17:46:30	930	210	0.09	0.03					488	
	MANA	17:47:21	981	270	0.2	0.05					440	